Multistable MOFs

DOI: 10.1002/anie.201204387

Hysteretic Three-Step Spin Crossover in a Thermo- and Photochromic 3D Pillared Hofmann-type Metal–Organic Framework**

*Natasha F. Sciortino, Katrin R. Scherl-Gruenwald, Guillaume Chastanet, Gregory J. Halder, Karena W. Chapman, Jean-François Létard, and Cameron J. Kepert**

The integration of spin crossover (SCO) centers into porous framework materials is leading to the emergence of new families of functional solids that display a range of interesting and potentially useful physicochemical properties. This materials design approach gives rise to a unique molecular scenario in which factors that govern the spin switching response (e.g., temperature, pressure, light, magnetic field, and chemical environment) are newly intertwined with highly cooperative structure–function relationships, and potentially also with the dynamic host–guest chemistry of the materials.[1–8] Among a range of such materials that exploit the ability of iron(II) to adopt either an $S=0$ low spin (LS) or an $S=2$ high spin (HS) state are a series of spin crossover frameworks (SCOFs) of general type $[Fe(L)_2(NCS)_2]$ (L = bis-unidentate ligand), which exhibit complex guest-dependent SCO behavior,[1–3,9] and a family of highly cooperative Hofmann-type materials $[Fe^{II}(L)M^{II}(CN)_4]\cdot x$guest (L = pyrazine or bispyridyl analogue; M^{II} = Ni, Pd, Pt)[4,5,7,8,10] and associated analogues,[8] which commonly display abrupt transitions with pronounced thermal hysteresis.

The role of cooperativity in SCO materials (i.e., the extent to which spin state changes are propagated in the solid state) has been widely investigated and is ascribed principally to elastic interactions between the spin switching centers.[11] Generally, for weakly cooperative systems, the SCO centers are considered effectively isolated, resulting in a gradual SCO behavior. Increasing the strength of the interactions, such as through the incorporation of covalent linkages, commonly leads to more abrupt transitions with thermal hysteresis (i.e., memory effects),[12,13] and, in relatively rare cases, to stepwise SCO behavior.[2,3,14] Multistep SCO materials[13,15] can be divided into two separate subclasses, the first in which the stepwise behavior results from the inherent structural inequivalence of the multiple SCO sites, and the second, more interestingly, where this inequivalence arises only in the intermediate phases. The latter are particularly important in providing insight into the nature of short-range interactions (steric and electronic)[14,16] and longer-range packing effects[2] that underpin lattice cooperativity, and in greatly extending the scope for application of SCO systems in areas such as data storage,[17] photo-responsive devices, molecular sensors, and all-photonics molecular computing.[13,18]

Recently, the first examples of three-step switching have been reported. The multicomponent system $[Fe(dpp)_2][Ni(mnt)_2]_2\cdot MeNO_2$ (dpp = 2,6-bis(pyrazole-1-yl)pyridine, mnt = maleonitriledithiolate)[19] displays three-step SCO on warming (HS fraction $0\rightarrow1/3\rightarrow2/3\rightarrow1$) following low-temperature dimerization of the $[Ni(mnt)_2]^-$ units (a transition that coincides in a single-step with SCO upon cooling). Three-step SCO has also been attributed to the 2D Hofmann-like network $[Fe(4\text{-methylpyridine})_2(Au(CN)_2)_2]$, for which the structure and composition of the intermediate states are unknown.[20] Here, we present a new 3D framework material $[Fe(dpsme)Pt(CN)_4]\cdot{}^2/_3\,dpsme\cdot x\,EtOH\cdot y\,H_2O$ (**1**; dpsme = 4,4′-di(pyridylthio)methane; EtOH = ethanol), which exhibits a three-step SCO transition that is unique in occurring both upon cooling and upon warming and in having broad thermal hysteresis. Accompanying this stepwise transition is a series of subtle structural modulations in which the material converts between different long-range configurations of ordered HS and LS sites.

The structure of **1** at 230 K, determined by using single-crystal X-ray diffraction (SCXRD), adopts the monoclinic *P*2/*a* space group (see Supporting Information for full crystallographic details). The asymmetric unit contains a single HS Fe^{II} center, which is N-coordinated equatorially to $[Pt(CN)_4]^{2-}$ and axially to dpsme. The material adopts the anticipated pillared Hofmann-type topology (Figure 1), in which 2D layers of $[FePt(CN)_4]$, consisting of cyanide-bridged alternating arrays of square-planar Pt^{II} and octahedral Fe^{II} sites, extend in the (001) plane and stack perpendicular to this. Bis-unidentate dpsme ligands bridge the iron atoms of adjacent layers (Fe···Fe distance 14.5 Å) to complete the open 3D Hofmann-type structure. The pillared topology generates rectangular channels along the [100] direction that account for 49% of the total crystal volume,[21] a value that is considerably larger than that of related Hofmann-type SCO materials.[22] These channels are occupied by disordered, non-coordinated dpsme ligands, which π-stack between the

[*] Dr. N. F. Sciortino, Dr. K. R. Scherl-Gruenwald, Prof. C. J. Kepert
School of Chemistry, The University of Sydney
Sydney NSW 2006 (Australia)
E-mail: c.kepert@sydney.edu.au
Dr. G. Chastanet, Prof. J.-F. Létard
Sciences Moléculaires, ICMCB, UPR CNRS 9048, Université Bordeaux I
87 Av. Du Doc. A. Schweitzer, 33608 Pessac (France)
Dr. G. J. Halder, Dr. K. W. Chapman
X-ray Science Division, Advanced Photon Source
Argonne National Laboratory, Argonne, IL 60439 (USA)

[**] Use of the Advanced Photon Source was supported by the U.S. Department of Energy, Office of Science, Office of Basic Energy Sciences, under Contract No. DE-AC02-06CH11357. N.F.S. thanks to the Australian Nanotechnology Network for financial support. K.R.G. thanks the Endeavour Research Fellowship for financial support.

Supporting information for this article is available on the WWW under http://dx.doi.org/10.1002/anie.201204387.

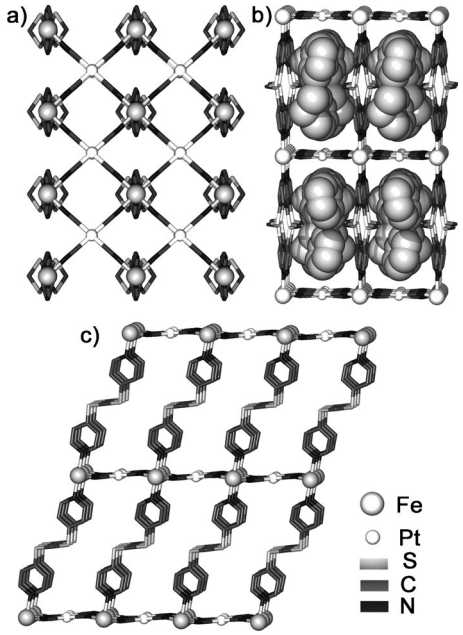

Figure 1. X-ray crystal structure of $[Fe(dpsme)Pt(CN)_4]\cdot{}^2/_3\,dpsme\cdot x\,EtOH\cdot y\,H_2O$ (**1**): a) view down the [102] direction, parallel with the dpsme pillars, showing the $[FePt(CN)_4]$ grid; b) 1D channels viewed down [100], occupied by dpsme ligand and solvent (space-filling); c) View down [010], showing the undulation and stacking of the 2D layers. Hydrogen atoms omitted in all figures, and guest molecules omitted in (a) and (c).

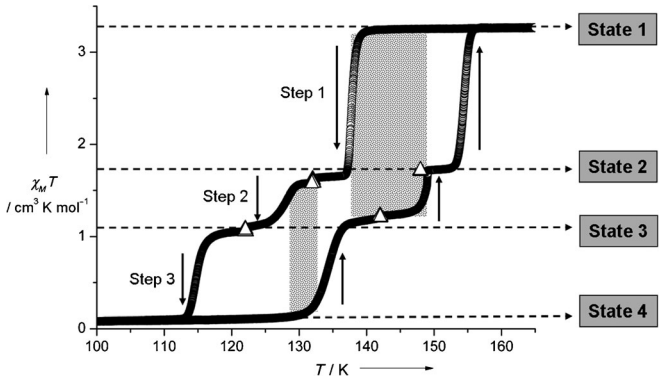

Figure 2. Temperature dependence of the molar magnetic susceptibility ($\chi_M T$) of **1**, displaying the complete three-step SCO behavior and ca. 20 K hysteresis (○). Relaxation of the $\chi_M T$ product over 1.5 h (△) during the plateau regions, indicating kinetic stability for the intermediate spin states. The shaded regions indicate temperature ranges over which the material exhibits tristability.

pyridyl units of the coordinated pillars, and disordered guest ethanol and water molecules. In contrast to previously reported, isotopological SCO phases, in which the use of rigid, linear pillars leads to highly symmetric structures having planar 2D $[M^{II}M'^{II}(CN)_4]$ layers,[4,7,23] the 3D Hofmann-type structure of **1** is notably distorted; at 230 K, the $[Fe^{II}N_6]$ octahedra are tilted by 7.89° out of the layer plane, generating a subtle undulation in the layers along [100] (Figure 1c).

Crystals of **1** display marked thermochromism associated with spin crossover behavior (Supporting Information, Figure S7), converting reversibly from yellow at room temperature to dark red at liquid nitrogen temperature due to the presence of the spin-allowed $^1A_1\rightarrow{}^1T_1$ d–d transition in the LS form. Figure 2 shows the thermal dependence of $\chi_M T$ ($\chi_M =$ molar magnetic susceptibility), confirming the presence of spin crossover and detailing stepwise behavior that occurs both upon cooling and upon warming. From room temperature to 140 K the $\chi_M T$ value remains approximately constant at ca. 3.30 $cm^3\,K\,mol^{-1}$, indicative of HS, $S=2$ Fe^{II} sites only. On further cooling, the $\chi_M T$ value decreases in three well-defined steps, to a minimum of 0.06 $cm^3\,K\,mol^{-1}$ below 110 K, consistent with exclusively LS, $S=0$ iron(II) sites. The first transition step, centered at 138 K, shows an abrupt drop to a plateau in the $\chi_M T$ values of ca. 1.54 $cm^3\,K\,mol^{-1}$, indicative of a spin state conversion in 50% of the iron(II) centers. The second and third transition steps, centered at 127 and 115 K, respectively, are also relatively abrupt and indicate successive spin conversions that complete the transition to fully LS Fe^{II} centers. With heating, a ca. 20 K hysteresis is revealed, with the three transitions now centered at 134, 148 and 154 K. To exclude the possibility of slow relaxation of the intermediate spin states, the temperature was held constant for 1.5 h at each plateau, which led to stable magnetic moments in all cases (Figure 2, △ data points). This behavior demonstrates that **1** undergoes a multi-stepwise spin transition according to the process:

State 1 [HS]←*Step 1*→*State 2* [1:1 HS:LS]←*Step 2*→*State 3* [ca. 1:2 HS:LS]←*Step 3*→*State 4* [LS].

Notably, the multiple steps are enclosed within a single thermal hysteresis loop, within which the intermediate states are retained when heating and cooling across the loop (*State 2* is stable with heating/cooling in the range 130 to 153 K and *State 3* from 117 to 148 K; see Supporting Information); as such, the behavior can be regarded as the partial overlap of three separate hysteresis loops, one for each crossover step. This unique behavior yields two separate regions over which the material exhibits tristability (*States 1*, *2* & *3* from 138 to 148 K and *2*, *3* & *4* from 127 to 134 K are each accessible through control of thermal history) and three of bistability (*States 1* & *2* from 148 to 154 K, *2* & *3* from 134 to 138 K, and *3* & *4* from 115 to 127 K). To our knowledge this represents the first formal demonstration of tristability in a SCO material, with it being common in the two-step systems for the hysteretic regions not to overlap.

In addition to thermal SCO, **1** displays light-induced switching properties. At low temperatures, irradiation of the LS state with green light (532 nm) induces a partial photoconversion to the HS state according to the LIESST effect.[24] At 10 K, this photo-induced HS state, which is kinetically stable in the dark, can be depopulated by irradiating at 830 nm according to the reverse-LIESST process (Figure 3b).[25] To our knowledge, this is the first example of a 3D Hofmann-type material displaying reversible photoswitching—a comparatively rare property to be reported among SCO materials in general. The stability of the photo-induced state in the absence of irradiation was determined by using a conventional T(LIESST) procedure.[26] Following an increase in $\chi_M T$ associated with zero-field splitting of the iron(II) centers, at 40 K the value of 2.75 $cm^3\,K\,mol^{-1}$

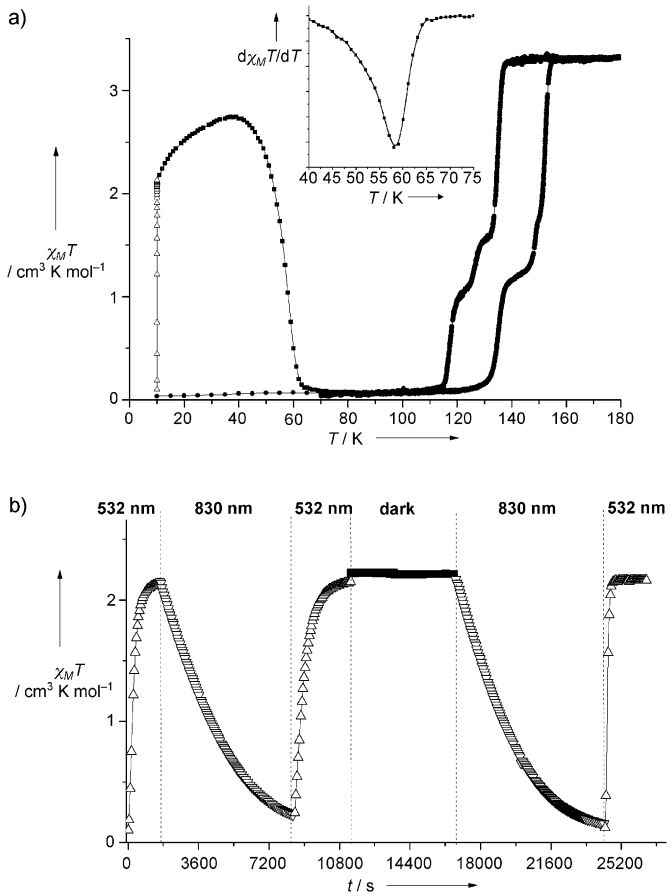

Figure 3. Photomagnetic data. a) Thermal dependence of the $\chi_M T$ product. ■: thermal spin crossover on warming and cooling; △: irradiation at 532 nm at 10 K; ●: thermal behavior in the dark of the photo-induced state. *T*(LIESST) corresponds to minimum of the derivative curve presented in the insert. b) Magnetic susceptibility response at 10 K under different wavelength irradiations (532 and 830 nm) in comparison to the time dependency recorded in the dark.

indicates a photoconversion yield of 83% (Figure 3a). Relaxation of the photo-induced state occurs above 50 K with a *T*(LIESST) temperature of 56 K (Figure 3a inset). In contrast to the thermal spin crossover, no steps or intermediate phases are evident in the *T*(LIESST) curve; a detailed study of the relaxation kinetics is ongoing to probe the presence of such intermediates phases in the photo-induced state lifetime.

To confirm phase homogeneity, thereby excluding the possibility that the crossover steps may arise due to sample polymorphism, and to investigate the mechanism behind the novel three-step SCO behavior, the structural consequences of the multistep switching were probed using synchrotron-based power X-ray diffraction (S-PXRD). Lattice parameters obtained from Le Bail fitting of the monoclinic parent cell to data collected over the temperature profile 230→90→230 K (Figure 4, Figures S9–S12) confirm single-phase behavior with pronounced discontinuous changes on cooling below 140 K. These changes lead to a 7.5% decrease in volume through three abrupt steps (Figure 4c). Consistent with the magnetic data, a thermal hysteresis of ca. 20 K is evident on warming, with the similarity of the patterns to those obtained on cooling confirming that the structure follows the same transition pathway. Close examination of the patterns revealed the brief existence of very weak diffraction peaks at low angles (e.g., 2.5°, (100); 3.3°, (101); 3.7°, (101)) that manifest between *Steps 1 & 2* of the spin transition; these indicate loss of the *a*-glide plane responsible for symmetry equivalence of the Fe sites in the parent HS structure (Figure 4b). Modulation peaks for *State 3* and peak-splitting associated with possible long-range reduction from the parent monoclinic to triclinic cells for *States 2 & 3* (see below) were not observed despite the low signal-to-noise and high resolution of the data (Figure S12).

From careful analysis of a large array of SCXRD data collected in succession over the profile 230→92→230 K, very subtle modulation peaks that were not present above and below the multistep crossover were found to appear concomitantly with *Steps 1–3* of the transition. This includes complex behavior in the vicinity of *State 3*, during which the modulation appeared to vary subtly with temperature. The outcome of full structural elucidation for each of the four states is illustrated in Figure 4d and is as follows. *Step 1*, [*State 1* (HS)↔*State 2* (1:1 HS:LS)], describes a lowering in symmetry from the parent monoclinic *P*2/*a* cell to a twinned triclinic $P\bar{1}$ solution of similar unit cell dimensions. Consequently, the single iron(II) site splits into two distinct iron(II) centers, Fe1 and Fe2, that respectively exhibit characteristic HS and LS coordination environments (mean bond lengths *d* [Å]: *State 1* Fe1–N 2.145; *State 2* Fe1–N 1.970, Fe2–N 2.171). Interestingly, the iron(II) sites are arranged in alternating rows of HS and LS within the Hofmann layer rather than in the more intuitive checkerboard arrangement, as observed in the two-step SCO material $[Fe(bpe)_2(NCS)_2]$ (bpe = 1,2-bis(4-pyridyl)ethane).[2] *Step 2*, [*State 2* (1:1 HS:LS) ↔ *State 3* (ca. 1:2 HS:LS)], involves a temperature dependent modulation along the *a*-axis in the triclinic lattice. Despite experimental difficulties inherent with maintaining a constant temperature and therefore modulation for this high pseudo-symmetry state, we were successful in collecting a full structural data set with very weak *a**/2 modulation peaks present throughout, corresponding to a doubling of the cell along *a*. The resulting structure contains two unique LS iron(II) centers (Fe1, site occupation factor (sof) 0.5; Fe2, sof 1) and a single unique HS iron(II) center (Fe3, sof 0.5) (mean bond lengths *d* [Å]: *State 3* Fe1–N 1.944, Fe2–N 1.991, Fe3–N 2.113), again with there being rows of HS and LS sites propagating along the *b*-axis, now in the form [LS–LS–LS–HS]. The observed HS:LS ratio of 1:3 is noticeably lower than that indicated by the magnetic data for the center of the *State 3* plateau, suggesting that a solid solution region with varying modulation along *a* may exist with conversion from a ca. 1:2 to a 1:3 HS:LS ratio, with the 1:3 phase being the most amenable to indexing and structural elucidation. *Step 3*, [*State 3* (ca. 1:2 HS:LS)↔*State 4* (LS)], reverts to the original parent cell in monoclinic *P*2/*a* (with no modulation), containing a single unique iron(II) site (Fe1) with a LS coordination environment (mean bond length *d* [Å]: *State 4* Fe1–N 1.954).

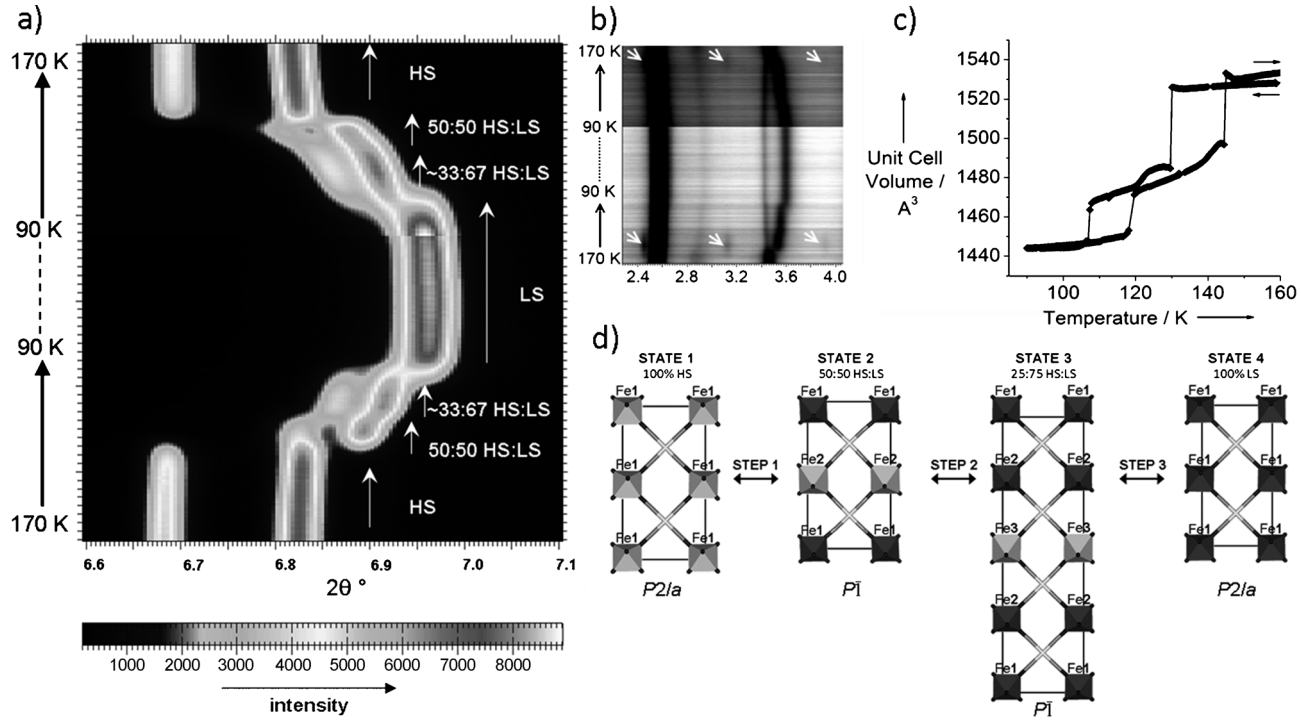

Figure 4. a) S-PXRD data peak intensity evolution versus temperature for **1** over the range 6.6–7.1°. Examination of the patterns reveals three clearly defined discontinuous structural transitions that occur concomitantly with *Step 1*, *Step 2* and *Step 3* of the SCO. b) Peak intensity evolution over the range 2.3–4.0° showing the brief existence of the modulation peaks (white arrows) corresponding to the monoclinic to triclinic symmetry lowering associated with *Step 1*. c) Evolution of the cell volume lattice parameter determined from the S-PXRD data. d) schematic of the $[FePt(CN)_4]$ framework component within the unit cell viewed down [001], illustrating the iron(II) spin state arrangement of HS (light gray) and LS (dark gray) sites associated with the structural transformation.

In addition to a progressive contraction of the structure that results from the decrease in Fe–N bond lengths with conversion from HS to LS, the increase in crystal field splitting energy with stepwise conversion to the LS state sees the adoption of a more regular framework geometry, with the FeN_6 octahedra tilted by only 3.30° out of the plane of the Hofmann layers in *State 4* (LS) compared to 7.89° in *State 1* (HS), and with the resulting more perpendicular alignment of the dpsme pillars being responsible for pronounced expansion along *c* (Figure S11). These changes see a progressive decrease in calculated pore volume; for *States 1*, *2*, *3* and *4* these are 766.1, 734.5, 718.5 and 707.1 $Å^3$ per formula unit, respectively, corresponding to 49.0, 48.1, 47.6 and 47.1% of crystal volume.[21] In light of these observations, we hypothesize that the multistep transition arises due to a subtle balance of host framework and host–guest energies, the former contributing multiple relative energy minima during thermal conversion between the HS and LS lattice states associated with the elastic cooperativity of the lattice (i.e., favoring abrupt conversion between distinct long-range configurations of HS and LS iron(II) sites) and the latter including what may be loosely regarded as an "internal pressure" term[4] associated with the progressive decrease in kinetic volume of the extraframework species with decreasing temperature; whilst there appears to be no obvious locking in of distinct guest configurations for each of the host framework spin states, the latter term may in principle help to stabilize each of these through the favorable matching of the temperature dependent guest and pore dimensions.

To conclude, we present a unique hysteretic three-step spin transition in a new pillared Hofmann-type framework material. X-ray diffraction analyses indicate that the four lattice spin states each adopt different long-range orderings of HS and LS sites, with subtle structural modulation yielding inequivalent iron(II) centers for the intermediate phases. The material is the first, to our knowledge, to exhibit such complex spin crossover behavior, the broad thermal hysteresis of which imparts two separate temperature ranges of tristability. Magnetic data indicate that each of the four lattice spin states are kinetically stable and accessible through thermal control, with photomagnetic measurements at low temperature yielding reversible interconversion between the LS and HS lattice states. The material provides a new platform for the examination of multistability in spin crossover systems, with perturbation of the lattice through chemical and other means likely to yield further insight into the novel behavior. Moreover, the external control of multistep switching in systems such as this opens intriguing prospects for application in a range of molecular devices.

Received: June 6, 2012
Published online: September 11, 2012

Keywords: Hofmann framework · metal–organic frameworks · molecular electronics · photophysics · spin crossover

[1] a) G. J. Halder, C. J. Kepert, B. Moubaraki, K. S. Murray, J. D. Cashion, *Science* **2002**, *298*, 1762 – 1765; b) S. M. Neville, B. Moubaraki, K. S. Murray, C. J. Kepert, *Angew. Chem.* **2007**, *119*, 2105 – 2108; *Angew. Chem. Int. Ed.* **2007**, *46*, 2059 – 2062; c) S. M. Neville, G. J. Halder, K. W. Chapman, M. B. Duriska, P. D. Southon, J. D. Cashion, J.-F. Létard, B. Moubaraki, K. S. Murray, C. J. Kepert, *J. Am. Chem. Soc.* **2008**, *130*, 2869 – 2876.

[2] G. J. Halder, K. W. Chapman, S. M. Neville, B. Moubaraki, K. S. Murray, J.-F. Létard, C. J. Kepert, *J. Am. Chem. Soc.* **2008**, *130*, 17552 – 17562.

[3] S. M. Neville, B. A. Leita, G. J. Halder, C. J. Kepert, B. Moubaraki, J.-F. Létard, K. S. Murray, *Chem. Eur. J.* **2008**, *14*, 10123 – 10133.

[4] P. D. Southon, L. Liu, E. A. Fellows, D. J. Price, G. J. Halder, K. W. Chapman, B. Moubaraki, K. S. Murray, J.-F. Létard, C. J. Kepert, *J. Am. Chem. Soc.* **2009**, *131*, 10998 – 11009.

[5] M. Ohba, K. Yoneda, G. Agustí, M. C. Muñoz, A. B. Gaspar, J. A. Real, M. Yamasaki, H. Ando, Y. Nakao, S. Sakaki, S. Kitagawa, *Angew. Chem.* **2009**, *121*, 4861 – 4865; *Angew. Chem. Int. Ed.* **2009**, *48*, 4767 – 4771.

[6] a) S. M. Neville, G. J. Halder, K. W. Chapman, M. B. Duriska, B. Moubaraki, K. S. Murray, C. J. Kepert, *J. Am. Chem. Soc.* **2009**, *131*, 12106 – 12108; b) M. B. Duriska, S. M. Neville, B. Moubaraki, J. A. Cashion, G. J. Halder, K. W. Chapman, C. Balde, J. F. Létard, K. S. Murray, C. J. Kepert, S. R. Batten, *Angew. Chem.* **2009**, *121*, 2587 – 2590; *Angew. Chem. Int. Ed.* **2009**, *48*, 2549 – 2552.

[7] R. Ohtani, K. Yoneda, S. Furukawa, N. Horike, S. Kitagawa, A. B. Gaspar, M. C. Muñoz, J. A. Real, M. Ohba, *J. Am. Chem. Soc.* **2011**, *133*, 8600 – 8605.

[8] M. C. Muñoz, J. A. Real, *Coord. Chem. Rev.* **2011**, *255*, 2068 – 2093.

[9] J. A. Real, E. Andres, M. C. Muñoz, M. Julve, T. Granier, A. Bousseksou, F. Varret, *Science* **1995**, *268*, 265 – 267.

[10] a) T. Kitazawa, Y. Gomi, M. Takahashi, M. Takeda, M. Enomoto, A. Miyazaki, T. Enoki, *J. Mater. Chem.* **1996**, *6*, 119 – 121; b) V. Niel, J. M. Martinez-Agudo, M. C. Muñoz, A. B. Gaspar, J. A. Real, *Inorg. Chem.* **2001**, *40*, 3838 – 3839.

[11] H. Spiering, *Top. Curr. Chem.* **2004**, *235*, 171 – 195.

[12] P. Gütlich, H. A. Goodwin, *Top. Curr. Chem.* **2004**, *233 – 235*; O. Kahn, C. J. Martinez, *Science* **1998**, *279*, 44 – 48.

[13] J.-F. Létard, P. Guionneau, L. Goux-Capes, *Top. Curr. Chem.* **2004**, *235*, 221 – 249.

[14] J. J. M. Amoore, C. J. Kepert, J. D. Cashion, B. Moubaraki, S. M. Neville, K. S. Murray, *Chem. Eur. J.* **2006**, *12*, 8220 – 8227.

[15] a) D. Chernyshov, M. Hostettler, K. W. Töornroos, H.-B. Bürgi, *Angew. Chem.* **2003**, *115*, 3955 – 3960; *Angew. Chem. Int. Ed.* **2003**, *42*, 3825 – 3830; b) M. A. Halcrow, *Polyhedron* **2007**, *26*, 3523 – 3576; c) J. Klingele, D. Kaase, M. H. Klingele, J. Lach, S. Demeshko, *Dalton Trans.* **2010**, *39*, 1689 – 1691; d) Ref. [14]; e) A. Bousseksou, G. Molnar, J. A. Real, K. Tanaka, *Coord. Chem. Rev.* **2007**, *251*, 1822 – 1833; f) A. B. Gaspar, M. C. Muñoz, J. A. Real, *J. Mater. Chem.* **2006**, *16*, 2522 – 2533; g) J. A. Real, I. Castro, A. Bousseksou, M. Verdaguer, R. Burriel, J. Linares, F. Varret, *Inorg. Chem.* **1997**, *36*, 455 – 464; h) J. A. Real, H. Bolvin, A. Bousseksou, A. Dworkin, O. Kahn, F. Varret, J. Zarembowitch, *J. Am. Chem. Soc.* **1992**, *114*, 4650 – 4658.

[16] A. Bousseksou, J. Nasser, J. L. K. Boukheddaden, F. Varret, *J. Phys. I* **1992**, *2*, 1381 – 1403; H. Romstedt, H. Spiering, P. Gütlich, *J. Phys. Chem. Solids* **1998**, *59*, 1353 – 1362.

[17] S. Bonhommeau, G. Molnar, S. Cobo, J. A. Real, F. Carcenac, E. Daran, C. Vieu, A. Bousseksou, *Adv. Mater.* **2007**, *19*, 2163 – 2167.

[18] a) A. P. de Silva, S. Uchiyama, *Nat. Nanotechnol.* **2007**, *2*, 399 – 410; P. Remón, M. Bälter, S. Li, J. Andréasson, U. Pischel, *J. Am. Chem. Soc.* **2011**, *133*, 20742 – 20745; b) G. Chastanet, C. Carbonera, C. Mingotaud, J.-F. Létard, *J. Mater. Chem.* **2004**, *14*, 3516 – 3523.

[19] M. Nihei, H. Tahira, N. Takahashi, Y. Otake, Y. Yamamura, K. Saito, H. Oshio, *J. Am. Chem. Soc.* **2010**, *132*, 3553 – 3560.

[20] T. Kosone, I. Tomori, C. Kanadani, T. Saito, T. Mochida, T. Kitazawa, *Dalton Trans.* **2010**, *39*, 1719 – 1721.

[21] Spek, A. L. *PLATON, A Multipurpose Crystallographic Tool*, Utrecht University, Utrecht, The Netherlands, **2010**.

[22] C. Bartual-Murgui, N. A. Ortega-Villar, H. J. Shepherd, M. C. Muñoz, L. Salmon, G. Molnar, A. Bousseksou, J. A. Real, *J. Mater. Chem.* **2011**, *21*, 7217 – 7222.

[23] G. Agustí, S. Cobo, A. B. Gaspar, G. Molnár, N. O. Moussa, P. Á. Szilágyi, V. Pálfi, C. Vieu, M. C. Muñoz, J. A. Real, A. Bousseksou, *Chem. Mater.* **2008**, *20*, 6721 – 6732.

[24] S. Decurtins, P. Gütlich, C. P. Kohler, H. Spiering, A. Hauser, *Chem. Phys. Lett.* **1984**, *105*, 1 – 4.

[25] A. Hauser, *Chem. Phys. Lett.* **1986**, *124*, 543 – 548.

[26] a) J.-F. Létard, L. Capes, G. Chastanet, N. Moliner, S. Letard, J.-A. Real, O. Kahn, *Chem. Phys. Lett.* **1999**, *313*, 115 – 120; b) J.-F. Létard, P. Guionneau, O. Nguyen, J. S. Costa, S. Marcen, G. Chastanet, M. Marchivie, L. Goux-Capes, *Chem. Eur. J.* **2005**, *11*, 4582 – 4589; c) J.-F. Létard, *J. Mater. Chem.* **2006**, *16*, 2550 – 2559.

